Monitoring the Optical/UV Transmission of the HRC with Betelgeuse

J. Posson-Brown, V. Kashyap

01 June 2005

Abstract

We have carried out a comprehensive analysis of all Betelgeuse calibration observations obtained to date with the HRC. Betelgeuse is undetected in all of the individual observations as well as cumulatively. We find that the expected exposure time for detection is > 1 Ms for aimpoint observations for both HRC-I and HRC-S, and therefore recommend discontinuing them. We also find that the predicted count rate due to the UV/optical flux is sufficient to have already resulted in a detection for observations carried out over the thin filter regions at large off-axis angles of the HRC-S. The non-detections therefore suggest that the out-of-band response must be decreased, by a factor < 0.3. We also recommend consolidating the observations over the outer wing plate into a single one at an off-axis angle of $-25'$.

1 Introduction

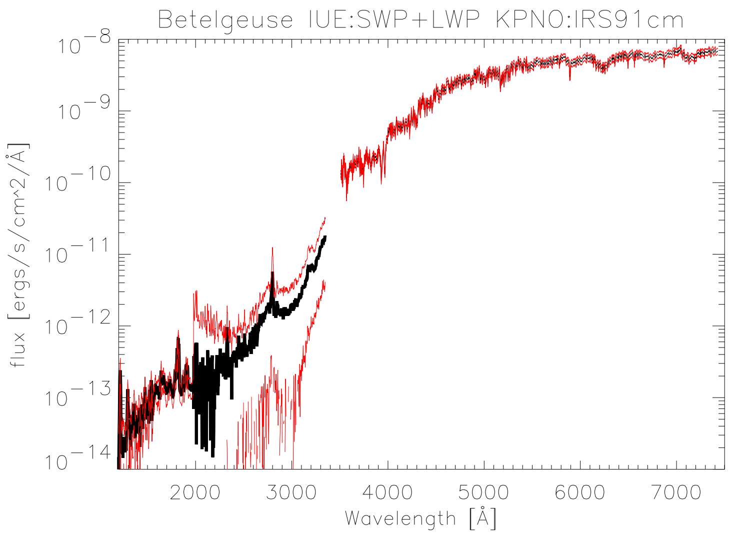

Figure 1: UV/optical spectral model for Betelgeuse. The UV part is derived from averaging its IUE spectra, and the optical part by normalizing standards spectra to its optical flux. The break at 3500Å is connected by linear interpolation. The statistical 1σ error band is shown in red.

Betelgeuse (α Ori, M1 Iab, $m_V = 0.58$, $B-V = 1.77$, $d = 131$ pc) is a red giant that has never been detected in X-rays. As the brightest red star in the sky, it is an ideal target to monitor the red leak and is therefore used as a regular *Chandra* calibration target to measure the transmission of the UV/ion-shield at long wavelengths. Figure 1 shows the UV and optical spectrum of Betelgeuse; the UV portion was derived by averaging all available *IUE* LWP and SWP large-aperture low-resolution spectra; and the optical portion was derived by averaging standard normalized M1 I and M2 I spectra from Jacoby, Hunter, & Christian (1984) and then scaling it to have the same optical flux as Betelgeuse. The standard deviation on the sample average is adopted as the error on the UV flux. For the optical flux, a constant 10% error as a function of wavelength is assumed, based on the differences between the standard spectra.

The two detectors which make up *Chandra's* High Resolution Camera (HRC) are shielded by aluminum-coated polyimide filters to reduce or block signals from UV light, ions, and low energy electrons. The UV/ion-shield (UVIS) over the HRC-I (aka the UVIS-I) is uniform: 5520Å of polyimide with 763Å of aluminum. The UVIS over the HRC-S (the UVIS-S) has segments with four different thicknesses (see Figure 2): a 2750Å-thick slab of polyimide over the central MCP, coated with 786Å-thick layer of Al over a 'T'-shaped segment covering the aimpoint (segment **1**), and a thinner 307Å layer of Al over the rest of the inner segment (segments **2**); a 2090Å slab of polyimide and a 304Å layer of Al over the spectroscopic dispersion region on the the outer plates (segments **3,4**), and a thicker 2125Å slab of polyimide and 1966Å layer of Al over the rest (segments **5,6**).

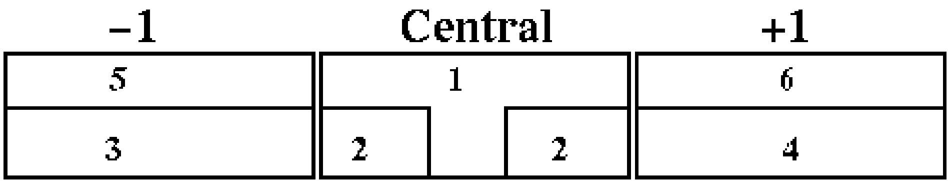

Figure 2: Sketch showing the arrangement of UVIS-S segments. Segments marked 1, 5, and 6 have larger thicknesses of polyimide and Al than segments marked 2, 3, and 4. The spacecraft Y-axis is aligned along the long axis and increases from right to left, while the Z-axis is aligned along the short axis and increases from bottom to top.

The current estimates of the response of the detector and filter to UV and optical light[1] are shown in Figure 3 for various combinations of interest (see also Zombeck 1999, Zombeck et al. 2000). The flux due to Betelgeuse is also shown. The expected count rate is dominated by the UV component of Betelgeuse's spectrum; despite the large intrinsic flux at long wavelengths, its contribution to the total count rate is generally more than an order of magnitude smaller than that due to the short wavelength flux.

Here we analyze all the HRC Betelgeuse observations to date to determine upper limits to its UV/optical flux, as well as the exposure times required to unambiguously detect it. We describe the observations in §2 and the analysis and results in §3. We summarize our conclusions in §4.

[1] For HRC-I and HRC-S respectively:
`http://hea-www.harvard.edu/HRC/calib/hrci_cal.html#uv_vis`
`http://hea-www.harvard.edu/HRC/calib/hrcs_cal.html#uv_vis`

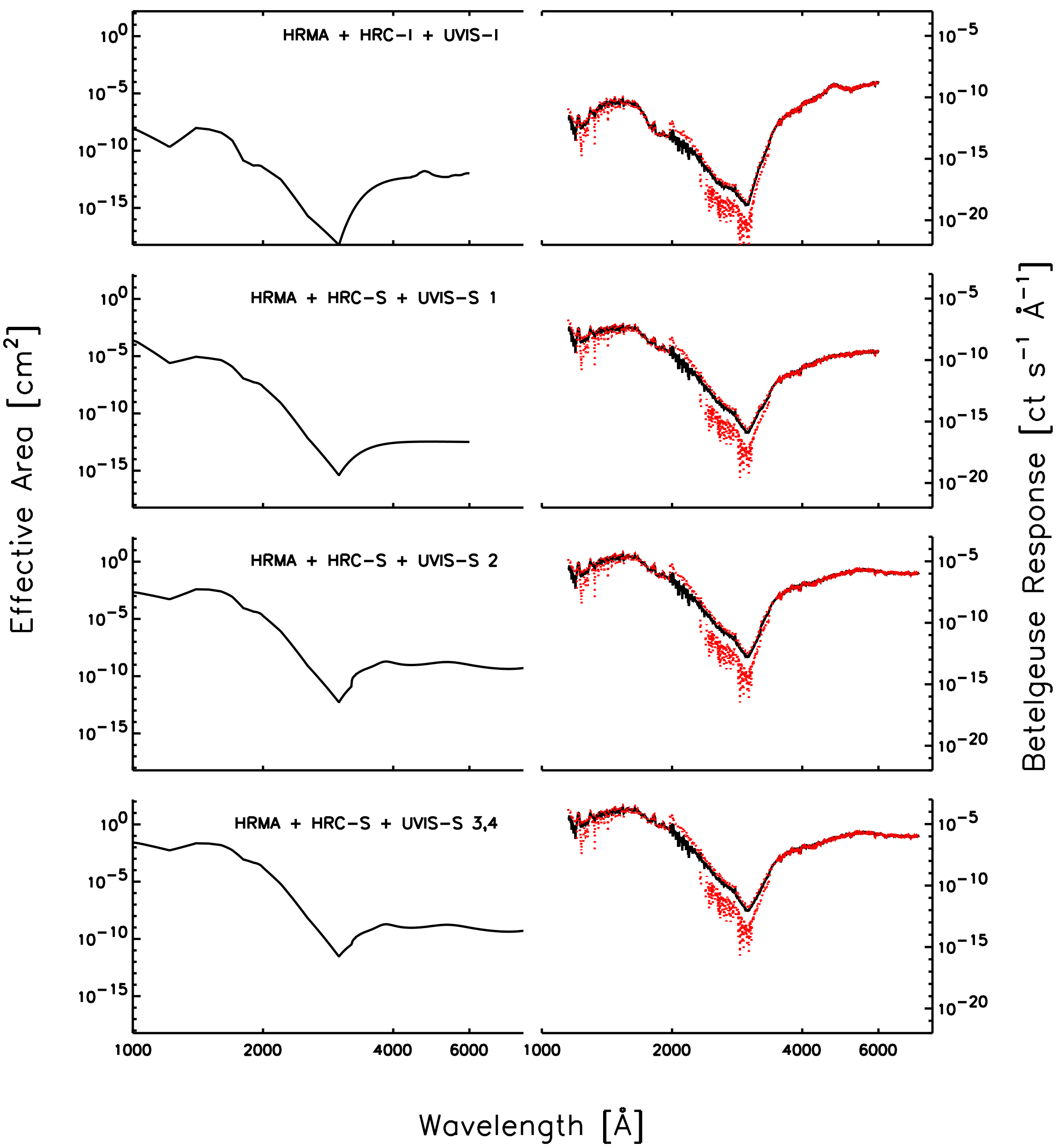

Figure 3: The HRC out-of-band effective area and the response to Betelgeuse. Each row of plots refers, sequentially, to data acquired under the filters (see Figure 2) UVIS-I, UVIS-S1, UVIS-S2, and UVIS-S3. (Note that UVIS-S3 is identical to UVIS-S4.) The figures to the left show the effective area; those to the right depict the predicted response of the detector to Betelgeuse. Note that despite the small intrinsic UV flux of Betelgeuse (Figure 1), the predicted count rate due to the UV leak is generally greater than to the red leak.

2 Data

Betelgeuse has been observed annually since 2001 to check for leaks in the UVIS. Each year, one HRC-I observation (at the aimpoint) and four HRC-S observations (one at the aimpoint and 3 off-axis) are carried out for ≈ 2 ks each. These observations are summarized in Tables 1 and 2.

Table 1: HRC-I observations of Betelgeuse. The listed exposure times are corrected for deadtime. Note that deadtime is not a concern for these observations, as the maximum count rate is < 146 ct s^{-1} (typically around 30 ct s^{-1}), which is safely under the telemetry saturation limit of 184 ct s^{-1}. All observations are carried out close to the nominal aimpoint, at $(Y,Z) = (0',0')$.

Date	ObsId	Exposure Time (s)
7 Dec 2001	2595	1892.10
6 Feb 2003	3680	1893.38
2 Feb 2004	5055	2075.88
2 Feb 2005	5970	2129.42

Table 2: HRC-S observations of Betelgeuse. Y offsets are along the dispersion axis and Z offsets are across the dispersion axis. As with the HRC-I data (Table 1), deadtime corrections are a minor factor, with the maximum count rate being < 170 ct s^{-1} (typically 40 ct s^{-1} for the wing plate and less than that for the central plate).

Date	ObsId	Exposure Time (s)	(Y, Z) Offset ($'$)
7 Dec 2001	2596	1926.67	0, 0
7 Dec 2001	2597	2167.22	-10, 0
7 Dec 2001	2598	1997.21	-20, 0
7 Dec 2001	2599	1297.95	-20, -3
6 Feb 2003	3681	1819.59	0, 0
6 Feb 2003	3682	2131.18	-10, 0
6 Feb 2003	3683	1903.91	-20, 0
6 Feb 2003	3684	2002.92	-20, -3
2 Feb 2004	5056	1945.28	0, 0
2 Feb 2004	5057	1467.02	-10, 0
2 Feb 2004	5058	1555.90	-20, 0
2 Feb 2004	5059	464.20	-20, -3
2 Feb 2005	5971	2140.42	0, 0
2 Feb 2005	5972	2148.69	-10, 0
2 Feb 2005	5973	998.37	-20, 0
2 Feb 2005	5974	1601.16	-20, -3

While the UV/ion shield is uniform over the HRC-I, it varies in thickness over the HRC-S to allow for increased sensitivity at different wavelength regions. A diagram of the UVIS-S is shown in Figure 2. Segment 1 is the thickest, with 2750Å of polyimide coated with 793Å of aluminum. This segment is monitored by observations of Betelgeuse at the aimpoint. Segment 2 is next thickest, with

2750Å of polyimide coated with 307Å of aluminum. This segment is monitored by observations done at $-10'$ off-axis. Identical segments 3 and 4 are the thinnest, with 2090Å of polyimide coated with 304Å of aluminum. These segments are monitored by observations done at offset locations $(Y,Z) = (-20',0')$ and $(Y,Z) = (-20',-3')$.[2] The identical segments 5 and 6, consisting of 2125Å of polyimide coated with 1966Å of aluminum, are not monitored by Betelgeuse observations.

Some of the off-axis observations on the HRC-S plates are affected by strong background flaring (see Figure 4). These times have been excised from the analysis, and the corrected exposure times are listed in Table 2. The exposure times also include corrections for instrument deadtime, though in all cases this is a minor effect: the peak count rate is always less than the telemetry saturation limit of 184 ct s^{-1}.

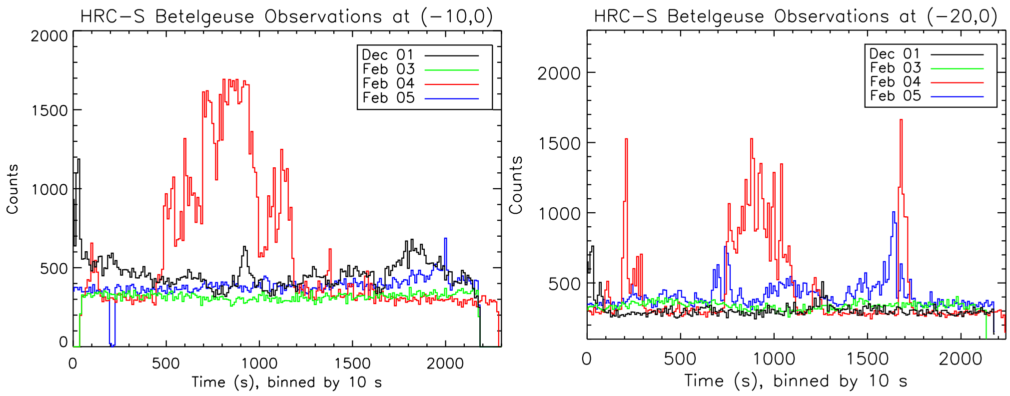

Figure 4: Lightcurves for data from entire chip for HRC-S observations of Betelgeuse prior to time filtering, at $(Y,Z) = (-10',0')$ (**left**) and at $(Y,Z) = (-20',0')$ (**right**). The start time has been reset for all observations to start from 0 for convenience. The Feb 04 data show large background flares; times thus affected have been excluded from the data during analysis. The lightcurves for the $(Y,Z) = (-20',-3')$ dataset show similar flaring, but have not been shown here in order to avoid cluttering the plot.

[2]The HRC-S is aligned such that the long axis, also the dispersion direction, is along spacecraft Y, and the cross-dispersion direction corresponds to Z.

3 Analysis

3.1 HRC-I+UVIS-I

As noted above, all HRC-I observations of Betelgeuse were carried out near the nominal aimpoint and monitor the UVIS-I. For each observation, we extracted counts from the level 2 event list in a $3.69''$ radius around the putative coordinates obtained from SIMBAD.[3] This corresponds to an enclosed energy of 98.7% of a point source (based on HRC-S Vega observations at the aimpoint) if such a source exists. We measure the background in an annulus of width $30''$ located $\sim 50''$ outside of the source region. We find that the background-subtracted net counts are consistent with no source detection (see Figure 5). We therefore compute the counts upper limit for detection, i.e., the the number of counts that, if seen, can be ruled out as arising due to the Poisson fluctuation of the background, at some suitable significance. The count rate upper limits based on a 99.7% confidence fluctuation (corresponding to a Gaussian-equivalent "3σ-detection") are also shown in Figure 5. We also compute the expected count rate due to the UV/optical flux in the HRC-I by folding the spectral model of Betelgeuse (see Figure 1) with a model of the detector's response to out-of-band radiation derived from pre-flight calibration measurements (Figure 3; see also Zombeck 1999, Zombeck et al. 2000). The expected count rates are much smaller than the upper limits derived from both the individual and co-added observations (see Table 4); indeed, it is practically impossible to obtain a detection of Betelgeuse with the HRC-I in the UV/optical during *Chandra*'s lifetime. We therefore recommend discontinuing the HRC-I Betelgeuse observations.

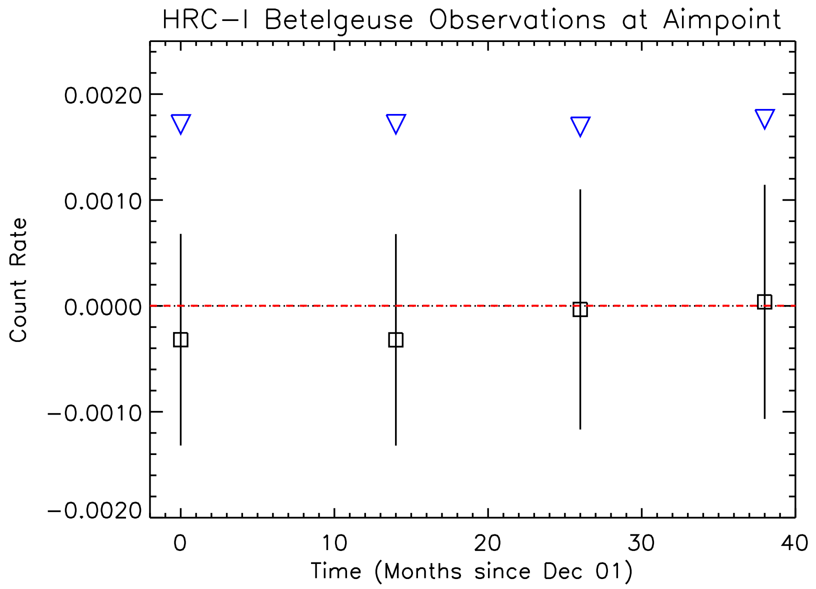

Figure 5: HRC-I+UVIS-I count rates for Betelgeuse. The background-subtracted estimates of the net source rates are shown (black squares) along with their estimated errors (solid vertical lines). The expected count rate due to the UV/optical flux from Betelgeuse is also shown as the red dashed line. The net count rates are consistent with there having been no detection. The upper limits computed at a 99.7% significance level are also shown (inverted triangles).

[3] http://simbad.harvard.edu/

3.2 HRC-S

3.2.1 UVIS-S1

Betelgeuse observations carried out at the HRC-S aimpoint sample the thick segment of the central MCP (segment 1 in Figure 2). For these data, we obtained the count rates using a method similar to that for the HRC-I (see §3.1). Source counts were extracted from a 3.69″ radius around the aimpoint (corresponding to a 98.7% enclosed count fraction, as determined from HRC-S aimpoint observations of Vega). Background counts were extracted from a 45″ wide annulus located 30″ outside the source region. As before, we find that the net count rates are consistent with zero (see Figure 6). We compute upper limits for a counts detection corresponding to a Gaussian-equivalent 3σ detection; these are also shown on the plot. These upper limits are large compared to the expected count rate (see Table 4), predicted by folding the spectral model of Betelgeuse (Figure 1) with the detector's response to out-of-band radiation derived from pre-flight calibration measurements (Figure 3). Based on this predicted count rate, we calculate that an exposure longer than 1 Ms would be needed to obtain an unambigous detection of Betelgeuse at the HRC-S aimpoint. In contrast, the accumulated exposure time for HRC-S aimpoint observations of Betelgeuse thus far is less than 8 ks. We therefore recommend discontinuing the aimpoint observations with the HRC-S as well.

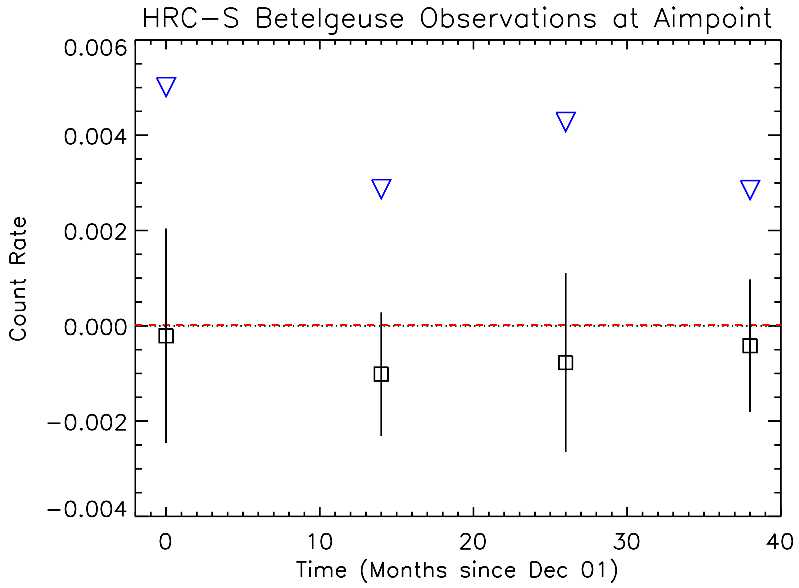

Figure 6: As in Figure 5, but for HRC-S data obtained at the aimpoint. These data sample segment 1 of the UVIS-S.

3.2.2 UVIS-S2

For Betelgeuse HRC-S observations at $-10'$, which sample the thin segment of the central plate (segment 2 in Figure 2), we used a method to determine the net source count rate that was similar to that used at the aimpoint, except for the sizes of the regions. Here, we use a 20.03″ radius for source count extraction (corresponding to a 98.0% enclosed count fraction, as determined from HRC-S observations of Vega at $-10'$) and a 45″ wide annulus located 60″ outside the source region for background counts. Again, as evident in Figure 7, we do not detect the source at this location and therefore compute upper limits at the Gaussian-equivalent 3σ level. We also do not detect the source in the co-added data. This non-detection is surprising, because the expected count rate in this region, ~ 0.012 ct s^{-1}, is sufficient to obtain a significant detection in 3.5 ks (see Table 4).

This is a robust result because of the simplicity of analysis (cf. §3.2.3) and the potential for detection, and can therefore be used to constrain the normalization of the HRC-S+UVIS-S2 response. We have carried out a Monte Carlo analysis to determine the correction factor, where we sample the source intensity from the *a posteriori* probability distribution function (see van Dyk et al. 2001) and compare it to the predicted counts calculated using the observed spectrum of Betelgeuse (Figure 1) and its response in the detector (Figure 3). We obtain 10,000 realizations of the ratio of calculated to expected source intensities, where in each iteration we also allow the counts obtained in the background region to vary according to the Poisson distribution and the predicted counts to vary according to the Gaussian distribution with a standard deviation determined from the observed error. The 68% confidence range of the correction factor, i.e., the factor by which the HRC-S+UVIS-S2 response must be decreased, is $0.036-0.3$ (see Figure 9). A better constraint on this number necessarily requires a detection of the source. A similar analysis of observations of Vega and other bright stars would then allow us to determine a wavelength dependent correction.

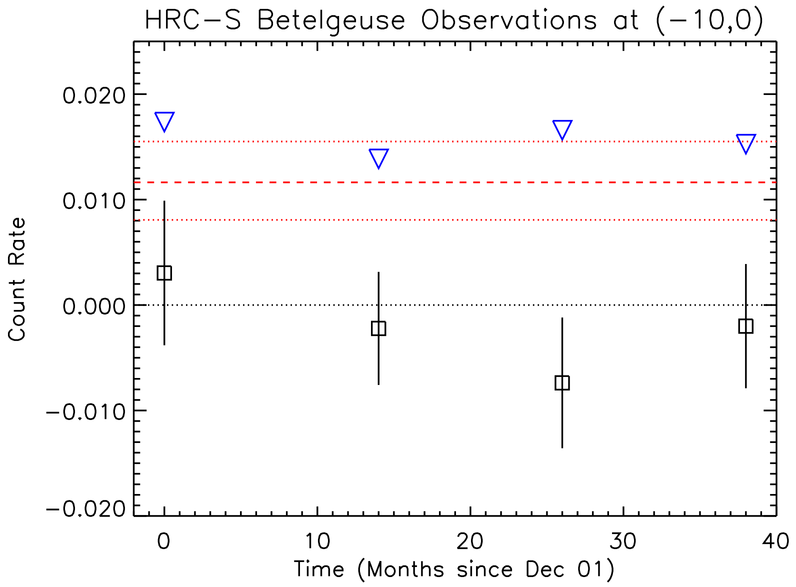

Figure 7: As in Figure 5, but for HRC-S data obtained at the offset pointing of $(Y,Z) = (-10',0')$. The error bars on the predicted count rate are also shown as red dotted lines. These data sample segment 2 of the UVIS-S.

3.2.3 UVIS-S3

The remaining two offset locations, at $(Y,Z) = (-20',0')$ and $(-20',-3')$ both sample segment 3 of the UVIS-S (Figure 2). We have therefore grouped these two sets of observations and analyzed them together. Note that these data sets were first filtered to remove time intervals that were dominated by background flares (see §2).

The observations in this set are located at the edge and corner of the negative wing plate. The point spread functions at these off-axis values are very large, and combined with the spatially varying background seen in the HRC-S (both along the Y and the Z axes), it is not possible to determine a local background level by considering counts in an annulus around the source location. We therefore adopted rectangular source regions covering the putative location of Betelgeuse, and for the background, used the same sized region over the same area of the detector, but for a different observation, and scale the background according to the exposure times and the expected background rate at the two observations. For the $(Y,Z) = (-20', 0')$ dataset, we measured the background from co-added, time-filtered, HRC-S non-grating observations of G21.5-09 (ObsID 1558; 10.5 ks), Vega (ObsID 32; 2.9 ks), and LMC X-1 (ObsID 1154; 2.2 ks); these observations are source-free in the region of interest. For the $(Y,Z) = (-20', -3')$ dataset, we used only ObsID 1154 to measure the background, as the other two observations (ObsIDs 32 and 1558) were done in a mode with edge-blanking, which excludes the putative source region at the corner of the plate. We adopt a source region of size $3.07' \times 1.65'$ for the $(Y,Z) = (-20', 0')$ observations, and a source region of size $3.07' \times 3.07'$ for the $(Y,Z) = (-20', -3')$ observations. Using HRC-S observations of Vega, we estimate that these regions enclose 76% and 78.5% of the nominal source counts respectively. We scaled the background counts by measuring the pure background at adjacent regions on the detector for the different observations, and then assuming that the ratio of these counts were the same over the source region. Betelgeuse is not detected in any of the observations individually, nor cumulatively (see Figure 8).

The expected count rate from Betelgeuse for this segment of the UVIS-S is $(3.33-7.85) \times 10^{-2}$ ct s^{-1}, which is comparable to the upper limits derived for the observations, and indeed, only 3.4 ks of exposure is required to obtain a significant detection (see Table 4). As with HRC-S+UVIS-S2 (§3.2.2), this affords us an opportunity to constrain the HRC-S+UVIS-S3 response. However, because of the difficulty in the analysis caused, first, by the loss of photons near the edge of the detector, and second, by the uncertainties involved in the background scaling, these results are of less significance. As before, we carry out a Monte Carlo analysis to determine the ratio of the observed to expected source intensities (see Figure 9). In this calculation we also include the uncertainty in the background scaling by constructing a set of scaling factors at numerous locations on the plate (away from sources), and sampling from these values randomly at each iteration. The ratios thus derived show a strong bimodal distribution (see Figure 9), and the 68% confidence ranges are $0.023-1.9$ at $(Y,Z) = (-20', 0')$ and $0.037-6$ at $(Y,Z) = (-20', -3')$. The bimodality in the probability distribution is an indication that either (a) the source is indeed detectable at these locations, but the systematic uncertainties in background determination can mask its detection, or conversely (b) that the background is subject to large uncertainties and can cause spurious detections of a source. These two mutually exclusive scenarios cannot be distinguished with the data at hand. In order to improve the quality of the analysis, we recommend consolidating the two sets of observations into a single observation at $(Y,Z) = (-25', 0')$.

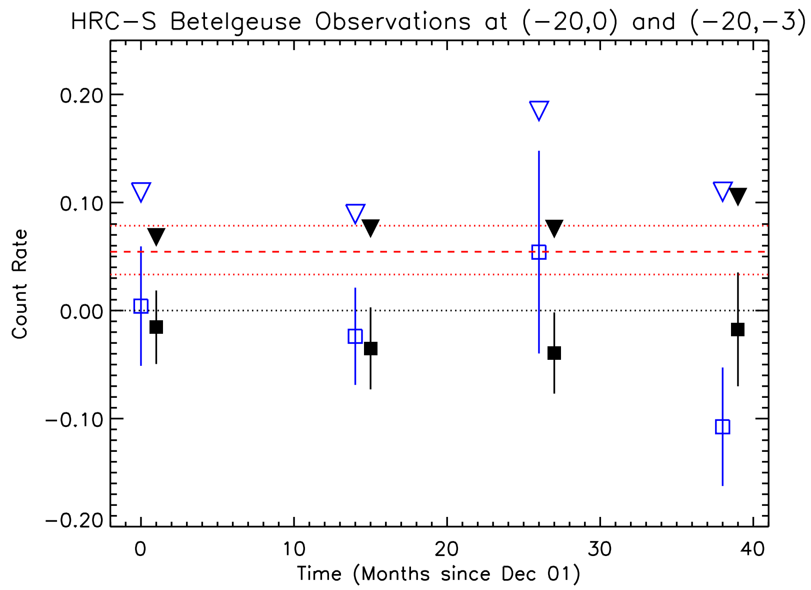

Figure 8: As in Figure 5, but for HRC-S data obtained at the offset pointing of $(Y,Z) = (-20', 0')$ and $(Y,Z) = (-20', -3')$. The former are denoted with filled symbols and the latter with open symbols, and are offset for clarity. The error bars on the predicted count rate are also shown as red dotted lines. These data sample segment 3 of the UVIS-S.

4 Conclusions

We have analyzed all the *Chandra* HRC observations of Betelgeuse to date. These observations were carried out in order to monitor the health of the UV/ion-shield of the HRC. The results of our analysis is summarized in Table 4.

In all cases, we find that Betelgeuse is undetected, individually as well as cumulatively.

We have calculated the expected count rates from the UV/optical flux of Betelgeuse at the aimpoint locations on the HRC-I and HRC-S, and have shown that the sensitivity of the observations is insufficient to detect it, both individually and cumulatively, in a reasonable time. An exposure time of $>$ 1 Ms is required to obtain a significant detection at these locations. Such exposure times will never be achieved during the course of regularly scheduled calibration observations over the lifetime of *Chandra*. **We therefore recommend that both HRC-I and HRC-S aimpoint observations of Betelgeuse be discontinued.**

In contrast, the expected rates at the off-center positions under the thinner segments of the UVIS-S are comparable to the computed upper limits, suggesting that the HRC-S+UVIS-S response must be revised downwards (see Figure 9).

The observations at $Y = -10'$ hold the best potential for a useful constraint and therefore **we recommend continuing these observations**.

The offset observations at $Y = -20'$ are subject to large systematic uncertainties due to their proximity to the edge of the negative wing plate and the difficulty in estimating the background within the source region. In order to facilitate the analysis, **we recommend that these observations be consolidated into a single pointing at** $(Y, Z) = (-25', 0')$, coincident with the position of the Vega observations.

Table 3: Summary of the HRC observations of Betelgeuse. The predicted count rates (and 1σ bounds) based on the UV/optical flux of Betelgeuse are compared with the upper limits derived from the accumulated data, and the time required for a detection at 99.7% significance is noted.

Filter	**Expected count rate** [ct s^{-1}]	**Accumulated Exposure** [s]	**Upper Limit** [ct s^{-1}]	**Required Exposure**
UVIS-I	$1.29^{+0.11}_{-0.14} \times 10^{-6}$	7991	7.04×10^{-4}	$>$ 1 Ms
UVIS-S 1 (center, thick)	$1.64^{+0.86}_{-0.71} \times 10^{-5}$	7832	1.86×10^{-3}	$>$ 1 Ms
UVIS-S 2 (center, thin)	$1.16^{+0.39}_{-0.36} \times 10^{-2}$	7914	7.86×10^{-3}	3.5 ks
UVIS-S 3,4 (outer, thin)	$5.44^{+2.36}_{-2.14} \times 10^{-2}$	11822	2.91×10^{-2}	3.4 ks

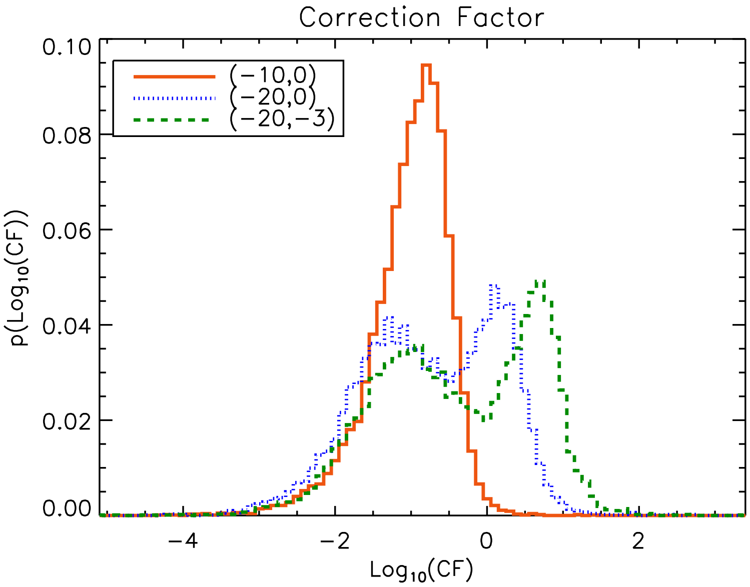

Figure 9: Probability distribution of the factor with which to correct the out-of-band HRC-S+UVIS-S response. The ratios of the observed to the predicted source intensities are generated during a Monte Carlo analysis that takes into account the errors in the measurements of the UV/optical flux, the counts in the background region, and the background-to-source scaling factors for the outer-wing data. The distributions for HRC-S+UVIS-S2 ($(Y,Z) = (-10', 0')$ – solid curve), and HRC-S+UVIS-S3 ($(Y,Z) = (-20', 0')$ – dotted curve; $(Y,Z) = (-20', -3')$ – dashed curve) are shown. The latter show a bimodal behavior that is due to the uncertainties inherent in the determination of a proper background rate at the locations of the source. The 68% confidence range on the correction factor, derived from the unimodal distribution of the correction factor for HRC-S+UVIS-S2, is $0.03-0.3$.

References

– Jacoby, G.H., Hunter D.A., & Christian C.A., 1984, ApJS, 56, 257

– van Dyk, D., Connors, A., Kashyap, V.L., & Siemiginowska, A., 2001, ApJ, 548, 224

– Zombeck, M., 1999, *CXC Memo*, `http://asc.harvard.edu/cal/Hrc/Documents/Zombeck/`

– Zombeck, M.V., Barbera, M., Butt, Y., Drake, J.J., Harnden, F.R.,Jr., Murray, S.S., & Wargelin, B., 2000, *X-Ray Astronomy 2000, Palermo*, `http://hea-www.harvard.edu/HRC/calib/palermopaper.ps`